

A Hybrid Deep Learning architecture for general disruption prediction across tokamaks

J.X. Zhu, C. Rea, K. Montes, R.S. Granetz, R. Sweeney, R.A. Tinguely

Massachusetts Institute of Technology, Plasma Science and Fusion Center, Cambridge, MA USA

Abstract: In this letter we present a new disruption prediction algorithm based on Deep Learning that effectively allows knowledge transfer from existing devices to new ones, while predicting disruptions using very limited disruptive data from the new devices. Future fusion reactors will need to run disruption-free or with very few unmitigated disruptions. The algorithm presented in this letter achieves high predictive accuracy on C-Mod, DIII-D and EAST tokamaks with limited hyperparameter tuning. Through numerical experiments, we show that good accuracy (AUC=0.959) is achieved on EAST predictions by including a small number of disruptive discharges, thousands of non-disruptive discharges from EAST, and combining this with more than a thousand discharges from DIII-D and C-Mod. This holds true for all permutations of the three devices. This cross-machine data-driven study finds that non-disruptive data is machine-specific while disruptions are machine-independent.

Introduction -- Nuclear fusion power delivered by magnetic-confinement tokamak devices holds the promise of sustainable and clean energy. The avoidance of sudden (usually unexpected) plasma terminations, called disruptions, within these devices is one of the most pressing challenges because their occurrence can halt power production and damage key components. Predicting plasma instabilities and disruptions from first-principle models has proven to be extremely difficult due to the complexity of the problem [1]. On the other hand, recent statistical and machine learning (ML) approaches based on experimental data have shown promising results for disruption prediction in real-time systems [2-10]. Different tokamak devices have different operational spaces, spatiotemporal scales for physics events and plasma diagnostics. Therefore, most of the previous approaches were developed and optimized specifically for one device and did not show promising cross-device prediction ability [2-6, 8, 10]. Specifically, cross-machine studies such as [7] focused on neural networks that were trained on datasets purely or mostly from one device: these predictors achieved great performances on the training device but lacked the generalization capabilities derived from an understanding of the underlying physics, and therefore tended to fail on new, unseen device data. This is a well-known problem which is called the shortcuts learning in the ML community. For instance, a neural network may appear to classify cows perfectly well—but it can fail when tested on pictures where cows appear outside the typical grass landscape, revealing “grass” as an unintended (shortcut) predictor for “cow” [11].

In this letter, we discuss a new Deep Learning (DL) application to disruption prediction that allows effective knowledge transfer from existing devices to new ones using very limited disruptive data from the new devices, while retaining high accuracy on the individual datasets. To this aim, we selected a set of disruption-relevant physical signals, available on all of the analyzed tokamak devices, and developed a powerful general algorithm using large databases from three tokamaks: Alcator C-Mod, DIII-D and EAST [8]. In addition, we combined data from the three different devices to add some randomization to the training domain which can alleviate over-learning of one specific device's behavior and designed a set of cross-machine experiments to find general guidelines for disruption prediction on new devices using very limited disruptive data from themselves. Moreover, unlike previous studies [7, 9-10], the three machines have very different features: EAST is a medium size ($R=1.85\text{m}$, $a=0.45\text{m}^1$) superconducting tokamak with a hybrid first wall, its lower divertor is in Carbon, the middle wall Molybdenum (Mo), while the upper divertor is made of Tungsten [12]. DIII-D is a medium size ($R=1.67\text{m}$, $a=0.67\text{m}$) tokamak with a carbon wall and relatively big error field: most of disruptive shots in our DIII-D database contain a locked mode as the

¹ R and a are respectively the major and minor radius of the toroidal device.

last precursor in their event chain toward disruption [13-14]. C-Mod is a small size tokamak ($R=0.68\text{m}$, $a=0.22\text{m}$) with high energy density (plasma pressure up to 2.05atm), high magnetic field (B_T up to 8T) and high-Z metal (Mo) wall. The combination of these different characters covers a substantial fraction of ITER's features [15-16]. A cross-machine study using data from these devices is well suited for investigating disruption prediction solutions for ITER.

The Hybrid Deep Learning (HDL) architecture -- Figure 1(a) shows the architecture of the hybrid neural network used for cross-machine disruption prediction. The network consists of two Gated Recurrent Unit (GRU) layers [17], one fully connected layer and three novel Multi-Scale Temporal Convolution (MSTConv) layers plus the input and the classification layer. The MSTConv layer is inspired from work in machine translation [18] and the detailed structure of one MSTConv layer is shown in Figure 1(b). It consists of six 1-D causal convolution layers [19] with different window lengths L from one to six. The first 1-D convolution layer can only access the current time step t_0 . The L-th 1-D convolution layer can look at L time steps from t_{0-L+1} to t_0 . This structure enables different 1-D convolution layers to capture local temporal information at different levels (1st order time derivative, 2nd order time derivative...). The resulting outputs from these six layers are concatenated and then processed through a batch normalization layer [20] and a ReLU activation to develop new features. It is important to highlight that different parts of the HDL architecture serve different purposes: The first two MSTConv layers are used to extract local temporal patterns from the input plasma sequences to form a richer representation of the input space. The following two GRU layers – with their long-term memory capability – can capture the long-range dependencies across different signals in the sequences. Then the following MSTConv and fully connected layers can compress and summarize the output representation from the GRU layers to a 12-dimension latent encoding² which can be mapped to the output by the classification layer.

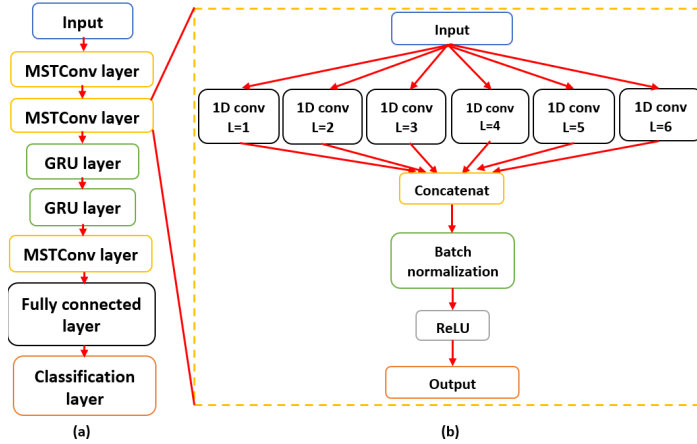


Figure 1: The HDL architecture (a) and the detailed structure of MSTConv layer (b). Notice that it consists of 6 1-D causal convolution layers with window lengths L from 1 to 6.

A shot-by-shot testing scheme was designed following [8] to simulate alarms triggered in the Plasma Control System (PCS), using the test shots from different devices. Given an input plasma sequence S (10x12 matrix), the predictor maps S to a 'disruptivity' between 0 to 1 at the last time step of the sequence where 1 is the disruptive class and 0 is the non-disruptive class. During testing, the whole flattop phase of each test shot is being subdivided in batches of 10 step sequences, given the HDL architecture design. Each neighboring testing sequence will have 9 steps overlap, and there are $N-9$ sequences for a test shot with N steps. If the disruptivity exceeds a preset threshold at any test time step, the test shot is classified as disruptive and the warning time is recorded for truly disruptive shots, defined as the difference

² The dimension of final latent space is a tunable hyperparameter.

between the alarm time and the final current quench. A successfully detected disruption on C-Mod is shown in Figure 2. Missing a real disruption or calling it too late (false negative, FN) is costly because its damaging effects go unmitigated, while triggering a false alarm (false positive, FP) wastes experimental time and resources, and may still damage the machine. Changing the alarm threshold value for the scalar disruptivity output of a prediction model allows a trade-off between these two factors. This trade-off is captured through a receiver-operator characteristic (ROC) curve [21]. The area under this ROC curve (AUC) measures the ability of the HDL predictor to catch real disruptions early enough, while at the same time causing few false positives. Throughout this paper, we describe the predictive performance on all tokamaks at **50 ms** before the disruption event: this is chosen as the minimum warning time for successful disruption mitigation on future devices [22].

The HDL predictor successfully achieves state-of-the-art performance on all three test sets (figure 3) comparable to other fully-optimized deep neural network disruption predictors [9]. To carry on a comparison with previous approaches to disruption prediction developed by the authors, we report the performance of the Random Forest (RF) predictors [6, 8] that are specifically optimized for each machine. The HDL predictor exceeds RF performances on all three datasets and shows the strong applicability and generalization power of the model. Besides its impressive performance, the inference time of our model is very short, allowing it to make a prediction in roughly 1ms using an 8-core CPU. This fast and novel model is not only an important step towards the prediction requirement of future devices, but also suggests a powerful conclusion. Although different devices may have disjoint operational regimes, there seems to exist a common type of discriminant function – same model hyperparameters - capable of separating the disruptive from non-disruptive phase on all these machines.

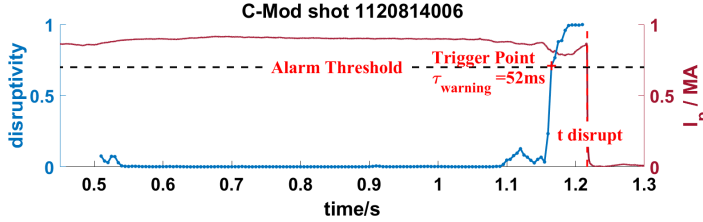


Figure 2: A successfully detected disruption on C-Mod.

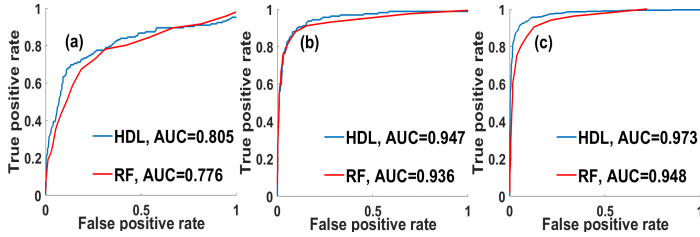


Figure 3: The ROC curves from test sets for HDL model and the Random Forest (RF) model, for C-Mod, DIII-D and EAST. (a) C-Mod; (b) DIII-D; (c) EAST.

Cross-machine study – The availability of a huge amount of experimental data across several tokamaks allows us to design numerical experiments to test transfer learning capabilities of the HDL architecture. Future reactors like ITER cannot withstand more than a few unmitigated disruptions [1], so we must be able to predict their disruptions given very limited disruptive data from themselves. It is tempting to verify *if and how useful* the data from existing devices is to be able to predict unstable plasmas on a new device. In the following section, we consider C-Mod and DIII-D as ‘existing machines’ and investigate the effect of their data for the HDL disruption predictor when used on EAST, chosen as a ‘new device’. However, **all following qualitative conclusions are machine-independent**: they always hold no matter which device is elected as the ‘new device’. The remaining two cases can be found in the supplementary material.

The first set of cross-machine experiments was conducted using limited disruptive training shots from the *new device*. The results of these experiments are shown in figure 4(a)-(b). In the first experiment, the disruption predictor was trained on 0.9% of all EAST disruptive shots (**20** randomly selected discharges) and all EAST non-disruptive data (5995 shots) plus all disruptive shots from C-Mod (929) and DIII-D (1049). This combination achieved the best performances on the EAST test dataset: AUC=0.959. In the second and third experiment, we first remove all EAST disruptive shots and then 50% of EAST non-disruptive shots from the first training dataset, separately. In the fourth experiment, the predictor was trained only using selected EAST data (20 disruptive shots, 5995 non-disruptive shots), this being our baseline model. In the fifth experiment, we add all non-disruptive shots from C-Mod and DIII-D to the first training dataset. In the sixth experiment, the predictor was trained only on DIII-D and C-Mod and its low performance highlights the importance of non-disruptive data from the target machine. From these numerical experiments, it is possible to draw the following conclusions:

1. HDL achieves relatively good performances on a new device if using a few disruptive shots and many non-disruptive shots from the new device plus many disruptive data from existing devices. All components mentioned above are necessary because removing any of them will decrease the performance (cases 1 to 4 in figure 4(a)).
2. Non-disruptive data from existing devices is harmful to HDL performance but disruptive data from existing devices improves the predictive power (cases 1, 4, 5 in figure 4(b)).
3. Non-disruptive data from the target device can substantially improve the predictive power (case 6 in figure 4(b)).

To further investigate the effect of the class imbalance in the training set, we conducted another set of experiments using all disruptive training shots of the new device. The results are reported in figure 5(a)-(b): Again, in the first experiment, the disruption predictor was trained on all EAST disruptive and non-disruptive shots, including all disruptive shots from C-Mod and DIII-D and it achieves the best performance on the EAST test dataset: AUC=0.983. In the second experiment, we add all non-disruptive shots from C-Mod and DIII-D to the first training dataset. In the third experiment, the predictor is trained only on EAST data which is a reference case for comparison. In experiments 4-6 (figure 5(b)), we randomly remove 2/3 of EAST non-disruptive training shots, thus reducing the non-disruptive training data to be less than disruptive training data, i.e. an inversely imbalanced situation. The test results from figure 5(a)-(b) point to the following further conclusions:

4. Adding disruptive data from existing machines can still improve test performances on the new device even though you have abundant new machine data (cases 1, 3 in figure 5(a)). However, adding non-disruptive data from existing machines is still harmful in this situation (cases 1, 2 in figure 5(a)).
5. The effects of disruptive data (positive) and non-disruptive data (negative) do not result from the class imbalance of the new machine dataset, because disruptive data from existing device continually has positive effects while the non-disruptive data still has negative effects in the inversely imbalanced situation (figure 5(b)). **This difference between disruptive and non-disruptive data is machine-independent**, i.e. a universal conclusion.
6. Also, removing non-disruptive data from the target device will always decrease the test performance no matter how imbalanced the target dataset is (cases 1, 3 in figure 4(a), case 6 in figure 5(b)).

Therefore, considering all the results above, disruptive data from existing devices can improve the performance on the new device while the non-disruptive data seems to have negative effects and these do not result from the label imbalance of training datasets. This suggests that the non-disruptive data is

specific to one device, but disruptive data contains some general knowledge about disruptions dynamics that could be transferred to a new device.

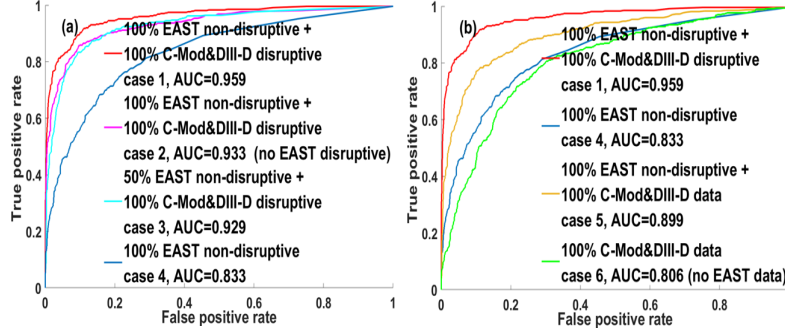


Figure 4: ROC curves from the EAST test set using 0.9% of EAST disruptive training shots. In figure (a), we show a curve (magenta) without any disruptive EAST training data, while in (b) we show a curve without any EAST training data (green).

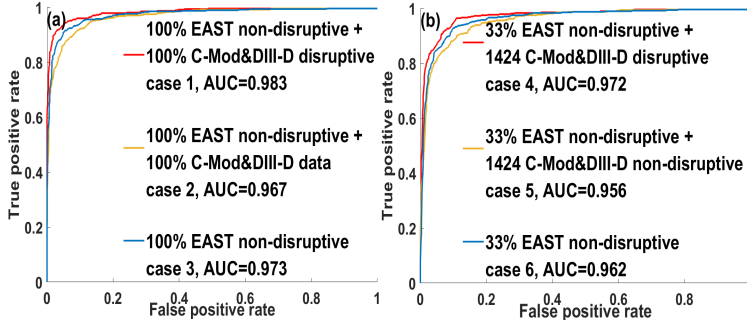


Figure 5: ROC curves from the EAST test set using 100% of EAST disruptive training shots. Figure (a) reports ROCs obtained including 100% non-disruptive EAST data, while (b) shows results when reducing to 33% the non-disruptive EAST training data.

Probability distributions of plasma signals for the different machines can be used to investigate the different features of non-disruptive and disruptive data. Figure 6(a) shows the distributions of non-disruptive poloidal beta (β_{pol}) signal on the three tokamaks, which exhibit clear differences across devices. The distributions of all other non-disruptive input signals show substantial distinction across different devices, too. This striking difference of the distributions of each individual non-disruptive signal across tokamaks reflects the fact that different devices have disjoint operational regimes. From the data-driven perspective, this further implies that finding a numerical transformation that maps a set of signals from DIII-D to EAST and vice versa is very challenging without incorporating machine-specific information, and this might indeed pose a great challenge when comparing ITER operational space to all existing devices. Due to all these considerations, we are inclined to conclude that non-disruptive data of existing devices is machine-specific and will only decrease the accuracy of the predictive models on the new device when it is directly mixed with data from the target device. Nevertheless, different devices show similar behavior when operating close to a disruption, as shown in Figures 6(b-d). The distributions of disruptive l_i signal on three machines exhibit a similar trend: a noticeable shift towards positive values, as the plasma gets closer to the disruption event. The plasma normalized internal inductance l_i will increase when a disruption is imminent, and it happens consistently on different tokamaks. We also observe similar behavior across the three different datasets for six (of twelve) input signals: $ip\text{-error}\text{-fraction}$, $locked\text{-mode}\text{-proxy}$, $v\text{-loop}$, β_{pol} , κ , $z\text{-error}\text{-proxy}$. These similar behaviors explain

the general knowledge about disruptions hidden beneath the disruptive data, which can be transferred to a new device.

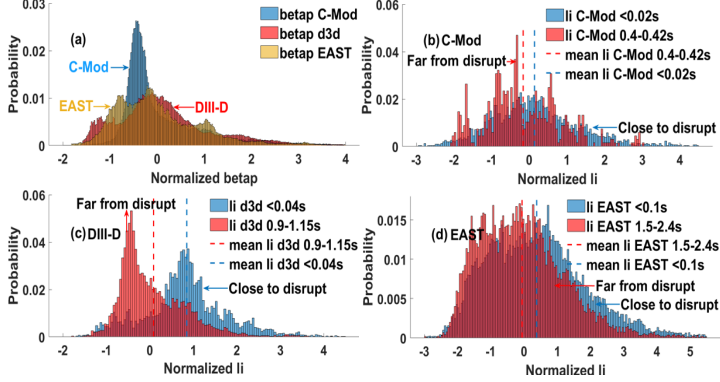


Figure 6: Distributions of plasma signals. (a) Non-disruptive betap signal on three machines; (b) disruptive li signal on C-Mod; (c) disruptive li signal on DIII-D; (d) disruptive li signal on EAST.

Summary and future plans -- In this letter, we have presented a new, powerful disruption prediction algorithm based on Deep Learning and also a general, effective way to transfer knowledge from existing devices to new devices which offers a guideline for disruption prediction on new devices using very limited disruptive data from target *new* devices. The cross-machine study on Alcator C-Mod, DIII-D, and EAST shows that the relatively good prediction performances on target devices can be achieved using a small set of disruptive shots while thousands of non-disruptive shots from themselves, and that such performances improve when including hundreds of disruptive discharges from other devices, no matter which device is chosen as the target *new* device. Furthermore, disruptive and non-disruptive data are found to have a different impact on the disruption prediction framework which implies that non-disruptive data is **machine-specific** and the disruptive data contains **general knowledge** about disruptions, and the distributions of plasma signals have been investigated to further support this conclusion. These results are an important milestone for disruption prediction research for next-generation burning plasma reactors, such as ITER. Future efforts will focus on two main topics. Firstly, the precision of our hyperparameter scan is limited by our computing power: Given enough computational resources, we can conduct a fine hyperparameter tuning which might increase the performance of the predictor and find new insights in the cross-machine study. Secondly, in the future version of HDL model we will explore how to directly incorporate device features such as minor radius, major radius, toroidal magnetic field, wall material, etc. The machine-specific character of non-disruptive data suggests that it could be beneficial to mix the device-specific representation with the plasma signal representation to increase the model's expressive power. This may enable us to extract information from machine-specific non-disruptive data and benefit the prediction on the new devices. We believe that the continuation of this project will let us contribute to the development of ITER disruption mitigation system, by designing a robust disruption prediction framework for ITER.

Acknowledgments -- This material is based upon work supported by the U.S. Department of Energy, Office of Science, Office of Fusion Energy Sciences, using the DIII-D National Fusion Facility, a DOE Office of Science user facility, under Awards DE-FC02-04ER54698 and DE-SC0014264. The HDL architecture reported in the paper was developed using TensorFlow library [23]. Part of the data analysis reported in this paper was performed using the OMFIT integrated modelling framework [24]. The authors are grateful to Nik Logan of PPPL; Earl Marmar of MIT; Richard Buttery and Chuck Greenfield of General Atomics for their support and valuable discussions.

Disclaimer -- This report was prepared as an account of work sponsored by an agency of the United States Government. Neither the United States Government nor any agency thereof, nor any of their employees, makes any warranty, express or implied, or assumes any legal liability or responsibility for the accuracy, completeness, or usefulness of any information, apparatus, product, or process disclosed, or represents that its use would not infringe privately owned rights. Reference herein to any specific commercial product, process, or service by trade name, trademark, manufacturer, or otherwise, does not necessarily constitute or imply its endorsement, recommendation, or favoring by the United States Government or any agency thereof. The views and opinions of authors expressed herein do not necessarily state or reflect those of the United States Government or any agency thereof.

Reference:

- [1] De Vries P. C. *et al.* 2016 *Fus. Sci. Technol.* **69**, 471–484
- [2] Wroblewski *et al.* 1997 *Nucl. Fusion* **37**, 725.
- [3] Cannas B. *et al.* 2004 *Nucl. Fusion* **44**, 68.
- [4] Murari, A. *et al.* 2008 *Nucl. Fusion* **48**, 035010.
- [5] Murari A. *et al.* 2018 *Nucl. Fusion* **58**
- [6] Rea C. *et al.* 2018 *Plasma Phys. Control. Fusion* **60**, 084004
- [7] Windsor C. G. *et al.* 2005 *Nucl. Fusion* **45**
- [8] Montes K. J. *et al.* 2019 *Nucl. Fusion* **59** 096015.
- [9] Kates-Harbeck J. *et al.* 2019 *Nature* **568**, 526–531
- [10] Rattá G. A. *et al.* 2018 *Fus. Sci. Technol.* **74**
- [11] Beery S. *et al.* 2018 *Proceedings of the European Conference on Computer Vision*, 456–473
- [12] Xu Y. *et al.* 2014 *Phys. Scr.* **2014** 014008
- [13] Turco F. *et al.* 2018 *Nucl. Fusion* **58** 106043
- [14] Sweeney R. *et al.* 2017 *Nucl. Fusion* **57** 016019
- [15] ITER Physics Basis Editors *et al.* 1999 *Nucl. Fusion* **39**
- [16] Ikeda K. *et al.* 2007 *Nucl. Fusion* **39**
- [17] Cho K. *et al.* 2014 *Eighth Workshop on Syntax, Semantics and Structure in Statistical Translation (SSST-8)*.
- [18] Lee J. *et al.* 2017 *Transactions of the Association for Computational Linguistics*, Volume **5**, 365-378
- [19] Oord A. V. D. *et al.* 2016 WaveNet: A Generative Model for Raw Audio
- [20] Ioffe S. *et al.* 2015 *Proceedings of the 32nd International Conference on International Conference on Machine Learning*, Volume **37**, 448-456
- [21] Bradley A. P. 1997 *Pattern Recognition*, **30**, 1145–1159.
- [22] Hollmann E. *et al.* 2015 *Physics of Plasmas* **22**

- [23] Abadi M. *et al.* TensorFlow: Large-scale machine learning on heterogeneous systems, 2015 tensorflow.org
- [24] Meneghini O. *et al.* 2015 *Nucl. Fusion* **55** 083008

Supplementary Material:

1. Dataset description

The choice of which parameters to include in the databases is guided by our knowledge of the plasma physics inherent in disruption phenomena, as well as the accessibility and consistency of these parameters on all three machines. Many of the disruption-relevant parameters included in this study are influenced by several papers published in literature [S1-S3]. The considered signals for the predictive models reported in this letter and their definition can be found in supplementary table 1, while the composition of the three training datasets is shown in supplementary table 2. Given these databases, we formalize the disruption prediction problem in a sequence-to-label supervised machine learning framework, where we assign a label to each example (**10** step consecutive sequence in time of **12** plasma signals) and train an algorithm to learn the functional representation mapping the input sequences to the assigned labels. To this aim, we explicitly defined different time thresholds for each machine to identify the unstable phase of the disruptive training discharges and assigned the *disruptive* label to plasma sequences that intersect the unstable phase of disruptive experimental runs, while the *non-disruptive* label is assigned to sequences extracted from the non-disruptive discharges. This classification scheme implicitly assumes that it is possible to detect a transition in time from a safe operational regime to a disruptive one and is another instance of incorporating physics knowledge into the AI workflow [S4-S5]. The chosen time thresholds vary on different considered devices which depend on the transition points where some of plasma parameters exhibit identifiable changes in behavior when disruptions occur vary on the three tokamaks, considering a notable fraction of disruptions [S6] and the suggestions from tokamak operators.

The training samples are ordered into sequences of ten time slices extracted from each shot of the training dataset. For each shot, we randomly select a subset of examples: this is a model's hyperparameter, tuned for each machine. The disruptive training sequences are randomly extracted from all sequences that intersect the unstable phase of each disruptive shot, while those sequences outside of the unstable region are not included in the training set. If disruptive patterns are learned properly, the algorithm will be able to identify similar trends also at times prior to the formally set time threshold, enabling the detection of early disruptive precursors. The non-disruptive sequences are randomly extracted from the flattop of non-disruptive training discharges. It is interesting to notice that that the database population consists in most non-disruptive data, thus resulting in a dataset imbalanced with respect to disruptive data.

Table 1: signals considered and their description

Signal description	Symbol
Plasma current – programed plasma current	
Programed plasma current	ip-error-fraction
Perburbed field of nonrotating mode^a	
($n = 1$ Fourier component), $B^{n=1}/B_{\text{tor}}$	locked-mode-proxy
Electron density	
Greenwald density	Greenwald-fraction
Distance between the plasma and the lower divertor	lower-gap
Current centroid vertical position error^b	z-error-proxy
Plasma elongation	kappa
Normalized plasma pressure (ratio of thermal to poloidal magnetic pressure)	betap

<u>Radiated power</u> <u>Input power</u>	radiated-fraction
Standard deviation of the magnetic field^c measured from an array of Mirnov coils, normalized by B_{tor}	rotating-mode-proxy
Loop voltage V_{loop}	v-loop
Safety factor at the 95% flux surface	q95
Normalized internal inductance	li

^aFor the C-Mod database, the locked-mode-proxy signal is obtained from a Mirnov coil array instead of the saddle coil.

^bFor the DIII-D database, we use current centroid vertical position instead of position error for the z-error-proxy signal.

^cFor the DIII-D database, we use n=1 component of magnetic field measured from a Mirnov coil array normalized by B_{tor} for the rotating-mode-proxy signal.

Table 2: The dataset composition of the three disruption warning databases

	Number of training shots	Number of test shots	Number of validation shots	Sampling Rate (ms)	Time Threshold (ms)	Number of samples per training shots
C-Mod	3343 (692 disruptive)	651	463	5	75	15
DIII-D	5286 (732 disruptive)	1085	734	10	400	25
EAST	8296 (2301 disruptive)	1674	1137	25	500	20

2. Algorithm and training details

Training the neural network effectively requires overcoming several unique challenges, such as the need for generalizable signal normalization, a need for increasing the transfer ability of the cross machine predictor, optimization of the hyperparameter, and a need for stabilizing the performance of the predictor. In this section, we will describe our approach to overcoming these challenges in our training procedure.

Normalization -- Neural networks typically expect all input features to lie in similar numerical ranges for all training examples [S7]. This poses a numerical challenge in the use of raw plasma signals as inputs to any neural network as different signals have values that can range over many different orders of magnitude. Furthermore, many signals will have differing characteristic scales on different tokamaks. Hence all 12 signals are normalized before being used in the network. The normalization should ideally be a common transformation such that maps signals with the same *physical meaning* from different machines onto the same numerical ranges after normalization. Different tokamak devices have different operational spaces, spatiotemporal scales and diagnostics. Moreover, different machines have different event chain toward disruptions and the most important disruption-relevant physics parameters are different on each machine. Therefore, such physics-based common transformation is hard to find and its extrapolation to ITER is uncertain. However, we find that the best-performing method is to standardize each signal on one machine by its mean and standard deviation across the entire dataset. For each signal on one machine, its normalized form is obtained as follows: $x_{\text{norm}} = (x - \text{mean}(x))/\text{std}(x)$. The normalization parameter sets of all considered signals on each machine can be found in supplementary table 3.

Table 3: Normalization parameters of each signal on three machines

Plasma signals	Mean EAST	Std EAST	Mean DIII-D	Std DIII-D	Mean C-Mod	Std C-Mod
ip-error-fraction	-0.0018	0.0206	-0.0157	0.0545	-0.0021	0.0425
locked-mode-proxy	0.0018	0.0037	$1.5462 \cdot 10^{-4}$	$3.5028 \cdot 10^{-4}$	$7.4951 \cdot 10^{-4}$	$4.3644 \cdot 10^{-4}$
Greenwald-fraction	0.4368	0.3270	0.4069	0.1840	0.2608	0.1315
lower-gap	0.1598 m	0.0321 m	0.1704 m	0.0823 m	0.0564 m	0.0163 m
z-error-proxy	0.0072 m	0.0222 m	$9.1142 \cdot 10^{-4}$ m	0.0059 m	$-8.4587 \cdot 10^{-7}$ m	0.0020 m
kappa	1.6298	0.1136	1.7675	0.1054	1.6176	0.0920
betap	0.6890	0.3795	0.8261	0.5011	0.2387	0.1839
radiated-fraction	0.1378	0.3470	0.5157	1.2370	0.3690	0.9520
rotating-mode-proxy	0.0049	0.0112	$6.8231 \cdot 10^{-5}$	$1.5536 \cdot 10^{-4}$	$0.6784 \cdot s^{-1}$	$1.0623 \cdot s^{-1}$
v-loop	0.4296 V	0.8612 V	0.2931 V	0.9360 V	-0.3294 V	1.7742 V
q95	6.0093	1.2748	4.8596	1.4172	4.4222	0.9427
li	1.1865	0.2280	1.0148	0.2148	1.4043	0.1720

The normalization process is independently done on all three machines which implies it is not machine-independent: a simple normalization scheme is instead chosen to solve the numerical challenge and leave the generalized signal transformation to the neural network. A machine-independent normalization method has also been tested for the three datasets: this normalization standardizes all datasets with a common set of parameters and gives slightly worse results. A performance comparison of HDL predictors using the two normalizations (machine-specific and machine-independent normalization) is shown in supplementary figure 1.

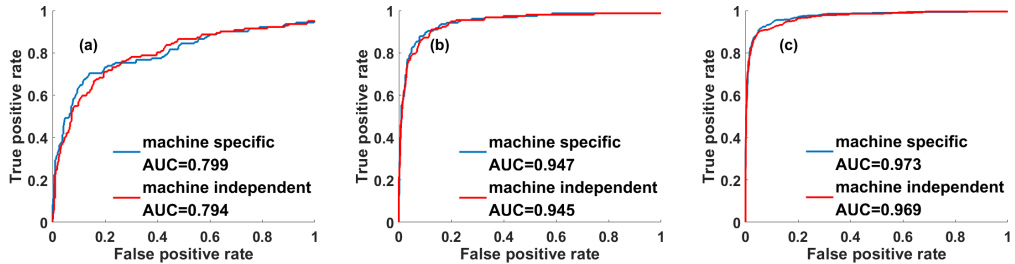


Figure 1: The ROC curves from test sets for machine specific normalization (blue) and machine independent normalization (red), for C-Mod (a), DIII-D (b), and EAST (c).

Cross-machine label smoothing -- In our cross-machine numerical experiments, we combine training data from different machines to form a new training set. However, direct mixing of data from various device can result in a problem: the initial assigned target labels for other devices might not suitable for the new test device. For example, a certainly disruptive sequence from EAST might not be that disruptive to C-Mod. Also, a non-disruptive sequence from C-Mod might be slightly unstable to EAST. In other word, you do not know what will happen if you run a C-Mod discharge on EAST or DIII-D and vice versa. To deal with

this problem, we choose two smoothing parameters ϵ_1, ϵ_2 for each device (ϵ_1 for non-disruptive examples and ϵ_2 for disruptive examples) and use these two parameters to modify the target value of the training examples from other machines. When we train the HDL predictor with part of the data from other machines, instead of using their initial (0, 1) target values for non-disruptive examples and disruptive examples, we modify their target values as $(\epsilon_1, 1-\epsilon_2)$ (The new target values for non-disruptive examples are ϵ_1 and the target values for disruptive examples are $1-\epsilon_2$. Notice that this modification is only applied to those training examples from other devices, those examples from the test device itself are not modified). We refer to this change in ground-truth target value as **cross-machine label smoothing** technique which can greatly improve the cross-machine ability of the HDL predictor.

Hyperparameter tuning and neural network ensemble -- The HDL disruption predictor has fourteen architectural and two labeling hyperparameters for each device. Guided by our previous numerical experiments on the C-Mod dataset, we scanned hyperparameters until finding a plateau where any hyperparameter set in this region gives high model performance. Within this region, changes in hyperparameters will only result in minor changes to the model's performance for all three devices. Outside this region, performance on at least one device starts to drop drastically. The hyperparameters of the HDL predictor are therefore selected from the middle of this region and all following qualitative cross-machine conclusions consistently hold for all hyperparameter sets in this plateau. Additionally, our approach includes the adoption of an ensemble of twelve neural networks, each one identical in their HDL architecture and tunable hyperparameters but with different initialization seeds: The final prediction comes therefore from an ensemble average. This method is popularly known in the ML community and shown to significantly improve the accuracy and stability of the predictor [S8-S10]. A comprehensive list of tunable hyperparameters for our HDL model can be found in supplementary table 4.

Table 4: Hyperparameters to be optimized, explanations and well-performing values

Hyperparameter	Explanation	Best Value
η	Learning rate	5×10^{-4}
beta2	The exponential decay rate for the second-moment estimates	0.970
N_{GRU}	Number of Gated Recurrent Unit (GRU) Layers	2
$n_{cells-1}$	Number of GRU cells in layer 1	130
$n_{cells-2}$	Number of GRU cells in layer 2	90
n_{batch}	Batch size	300
Target	Type of target function	Negative Log-Likelihood (NLL)
N_F	Number of convolutional filters in the 1-D causal convolution sublayers of each Multi-Scale Temporal Convolution (MSTConv) layer	10
Optimizer	Stochastic optimization scheme	Adam
Dropout	Dropout probability	0.1
L2 regularization	Weight regularization of all weight	1×10^{-3}
n_{epoch}	Number of training epochs	32
d_{latent}	Dimension of final latent representation	12
$N_{MSTConv}$	Number of MSTConv Layers	3
$\epsilon_{1-C-Mod}$	Smoothing parameter ϵ_1 when test on C-Mod	0.00
$\epsilon_{2-C-Mod}$	Smoothing parameter ϵ_2 when test on C-Mod	0.08
$\epsilon_{1-DIII-D}$	Smoothing parameter ϵ_1 when test on DIII-D	0.00
$\epsilon_{2-DIII-D}$	Smoothing parameter ϵ_2 when test on DIII-D	0.05

ε_1 -EAST	Smoothing parameter ε_1 when test on EAST	0.09
ε_2 -EAST	Smoothing parameter ε_2 when test on EAST	0.00

3. Cross-machine numerical experiments using C-Mod and DIII-D as target devices

Cross-machine experiments testing on C-Mod -- In these experiments, we consider EAST and DIII-D as ‘existing machines’ and investigate the effect of their data for the HDL disruption predictor when used on C-Mod, chosen as a ‘new device’. The numerical results are shown in supplementary figure 2-3 which consistently support our previous cross-machine conclusions, to be found in Section 3, cross-machine study.

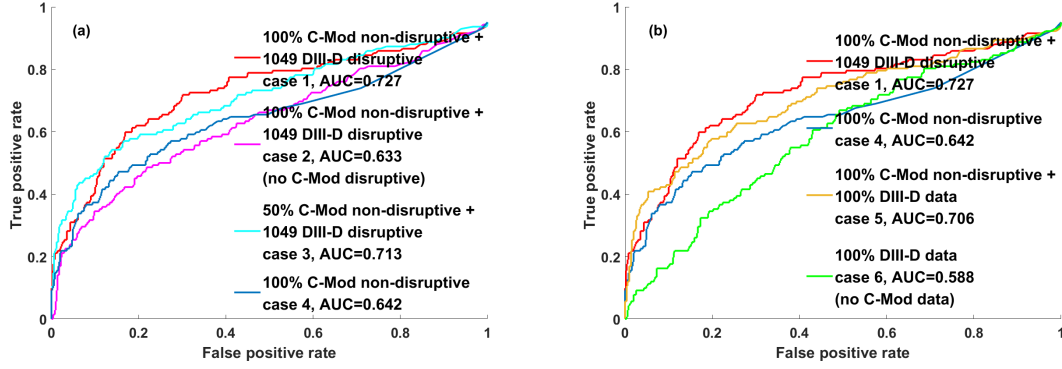


Figure 2: ROC curves from the C-Mod test set using 20 C-Mod disruptive training shots (2.9%). In figure (a), we show a curve (magenta) without any disruptive C-Mod training data, while in (b) we show a curve without any C-Mod training data (green).

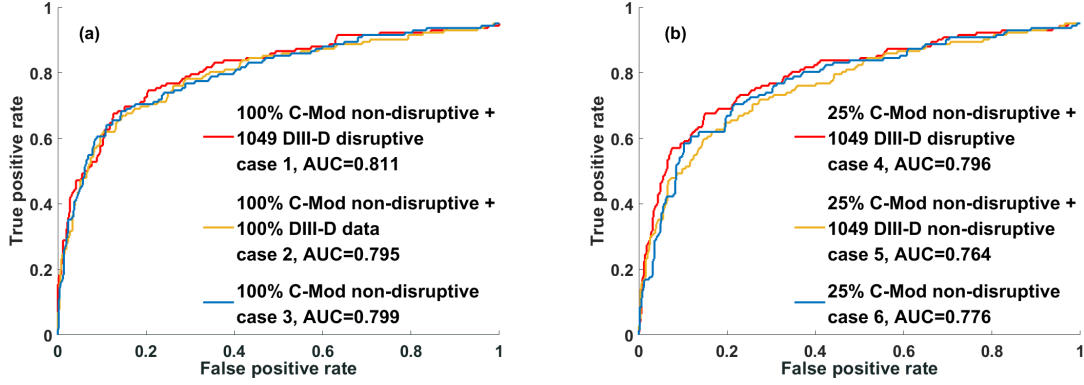


Figure 3: ROC curves from the C-Mod test set using 100% of C-Mod disruptive training shots. Figure (a) reports ROCs obtained including 100% non-disruptive C-Mod data, while (b) shows results when reducing to 25% the non-disruptive C-Mod training data.

Cross-machine experiments testing on DIII-D -- In these experiments, we consider EAST and C-Mod as ‘existing machines’ and investigate the effect of their data for the HDL disruption predictor when used on DIII-D, chosen as a ‘new device’. The numerical results are shown in supplementary figure 4-5 which consistently support our previous cross-machine conclusions, to be found in Section 3, cross-machine study.

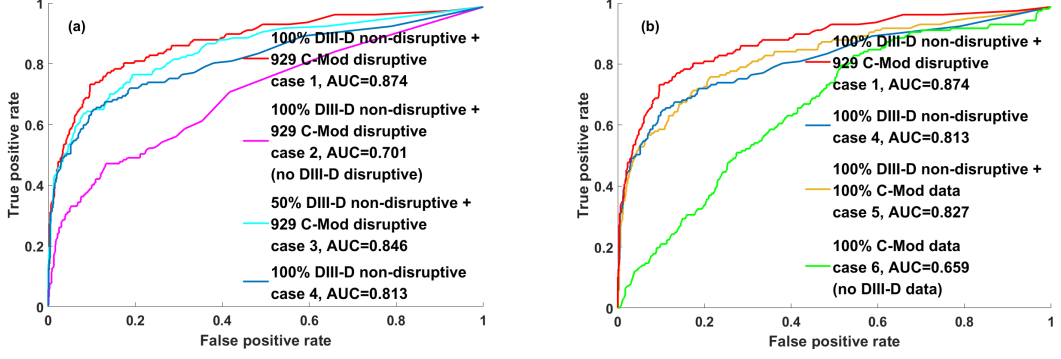


Figure 4: ROC curves from the DIII-D test set using 20 DIII-D disruptive training shots (2.7%). In figure (a), we show a curve (magenta) without any disruptive DIII-D training data, while in (b) we show a curve without any DIII-D training data (green).

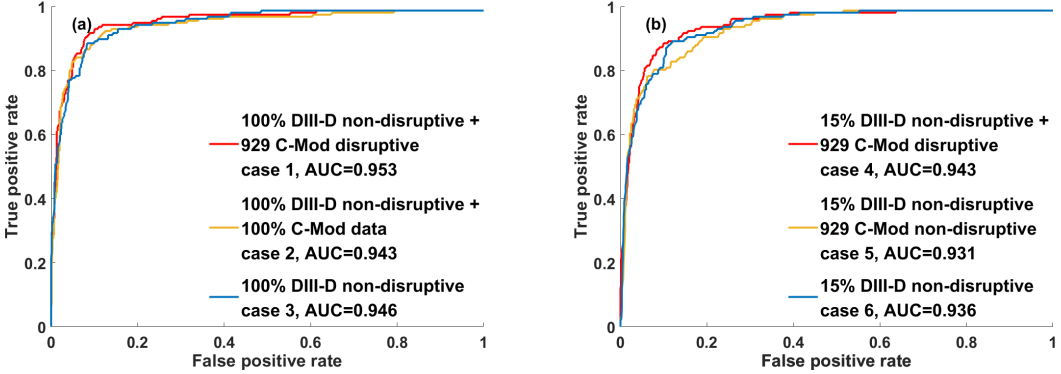


Figure 5: ROC curves from the DIII-D test set using 100% of DIII-D disruptive training shots. Figure (a) reports ROCs obtained including 100% non-disruptive DIII-D data, while (b) shows results when reducing to 15% the non-disruptive DIII-D training data.

Supplementary Reference:

- [S1] Gerhardt S. *et al.* 2013 *Nucl. Fusion* **53**
- [S2] Cannas B. *et al.* 2007 *Nucl. Fusion* **47** 1559
- [S3] Vega J. *et al.* 2013 *Fusion Eng. Des.* **88** 1228
- [S4] Rea C. *et al.* 2019 *Nucl. Fusion* **59** 096016
- [S5] Pau A. *et al.* 2019 *Nucl. Fusion* **59** 106017
- [S6] Montes K. J. *et al.* 2019 *Nucl. Fusion* **59** 096015.
- [S7] Goodfellow, I. 2016 *Deep Learning*, MIT Press, Cambridge, MA
- [S8] Haykin, S. 1999 *Neural Networks: A Comprehensive Foundation*. 2nd Edition, Prentice Hall, Englewood Cliffs, NJ
- [S9] Hansen L. K. *et al.* 1990 *IEEE Trans. Pattern Anal. Machine Intell* **12** 993-1000
- [S10] Perrone M. *et al.* 1993 *Neural Networks for Speech and Image Processing*, R. J. Mammone, Ed. London, U.K